Author‘s Manuscript - Public Access

Max-Planck-Institut für Polymerforschung
Max Planck Institute for Polymer Research

Published in final edited form as:

Teisala, H., Schönecker, C., Kaltbeitzel, A., Steffen, W., Butt, H.-J., & Vollmer, D. (2018). Wetting over pre-existing liquid films. Physical Review Fluids, 3(8): 084002. doi:10.1103/PhysRevFluids.3.084002.

Wetting over pre-existing liquid films

Teisala, H., Schönecker, C., Kaltbeitzel, A., Steffen, W., Butt, H.-J., & Vollmer, D

This article may be used for non-commercial purposes in accordance with publisher’s Terms and Conditions for Self-Archiving.

Max Planck Institute for Polymer Research – Author's Manuscript

Wetting over pre-existing liquid films

Hannu Teisala, Clarissa Schönecker, Anke Kaltbeitzel, Werner Steffen, Hans-Jürgen Butt*, Doris Vollmer

Max Planck Institute for Polymer Research
Department of Physics at Interfaces
Ackermannweg 10
D-55128 Mainz, Germany

*Corresponding author: Hans-Jürgen Butt (butt@mpip-mainz.mpg.de)

Keywords: wetting, meniscus, hydrodynamics, Laplace pressure, capillary, surface tension, lubricant, slippery surface

Abstract

Wetting of a liquid over another, pre-existing liquid film governs several natural phenomena and technical applications such as coating and oil recovery. The dynamics of this everyday process are poorly understood due to the lack of space and time resolved techniques, which can discriminate between the two liquids. Here we image a water front moving on a micrometer thick film of a solid supported silicone oil using laser scanning confocal microscopy. The silicone oil forms a meniscus around the water front. We resolve the spreading dynamics within the meniscus in 3D using tracer microparticles. Capillary suction induces local thinning of the oil film adjacent to the meniscus. When moving the water front forward, viscous forces deform the oil meniscus, giving rise to a wave-like film profile with local backflows. For high velocities, the film profile can be modeled within the Landau-Levich-Bretherton framework. The theory fails to predict the film profile at low velocities where strong capillary-suction-induced backflows occur.

Max Planck Institute for Polymer Research – Author's Manuscript

I. Introduction

Controlling the wetting properties and film formation are of utmost importance in many fields of technology including coating and printing applications [1-4], assembly of colloidal particles [5], lubrication of surfaces and bearings [6], oil recovery [7], flotation to recycle and enrich minerals [8], and fabrication of self-cleaning or water repellent surfaces [9-16]. These processes are dynamic – and often greatly influenced by menisci, i.e. a curved liquid interface that forms when a liquid meets a solid or another, immiscible liquid [17]. Liquid films also are important in many biological systems. Instructive examples are a human eye [18,19] where the tear film on cornea is stabilized by menisci at the eye lids or *Nepenthes* pitcher plants [20] where the prey capture mechanism is based on aquaplaning of insects at the slippery peristome.

Dynamic wetting of one liquid over a solid supported thin film of another, immiscible liquid is still hardly explored [21]. This lack of knowledge is due to missing experimental techniques which are able to discriminate between different liquids or provide the required time and spatial resolution. Wetting over liquid films has become increasingly important due to the innovation of lubricant-infused slippery surfaces [22-29] – a new class of functional materials inspired by the pitcher plant [22,29]. Liquid drops slide on a solid supported lubricant film at very low tilt angles, typically even below 3° [23,28]. Schellenberger et al. [25] showed that in equilibrium, the meniscus around a drop on a lubricant-infused surface can reach the length of ~3 mm. So far, flow dynamics within menisci and the film region ahead of moving drops remain unknown.

Here, we investigate water front advancing over a thin, pre-existing film of silicone oil on a smooth glass surface. At the liquid contact line the oil is elevated to a meniscus (Fig. 1 and

Max Planck Institute for Polymer Research – Author's Manuscript

Fig. S1a). The meniscus is pushed forward by the advancing water front. We apply laser scanning confocal microscopy to image the shape of all liquid interfaces. Surprisingly, the meniscus is not monotonous but shows wave-like profile with local minima and maxima. We quantify the spatial and temporal variation of the Laplace pressure in the oil. We quantify the local pressure gradient driven backflows in the meniscus and the film by adding 1 µm diameter polystyrene tracer particles to the oil. This capillary-suction-induced flow in the meniscus is universal and can last even for days. Due to the design of our setup, the shape of the meniscus is not disturbed by gravity. This allows us to investigate low capillary numbers. We analyze the shape of the liquid interface using the lubrication approximation, balancing viscous and capillary forces. The theory cannot predict the film profile for $Ca = \eta\, v/\gamma < 6\times10^{-4}$, as no single wavelength can be defined. Here, η is the viscosity of the oil, v the velocity of the meniscus, and γ the oil–air surface tension.

II. Results

We first observe a situation where a 0.5 µL water drop is placed on a smooth glass substrate coated with a film $h_0 \approx 10$ µm of silicone oil (polydimethylsiloxane, PDMS, η = 50 mPa s, γ = 21 mN/m), Fig. 1a,b. The silicone oil forms a wetting ridge, i.e. a concave curved annular meniscus, around the drop. Adjacent to the meniscus the film is depleted and a local minimum film thickness $h_{min} \approx 1$ µm forms before the film reaches its initial thickness $h_0 \approx 10$ µm far away from the meniscus.

The depletion zone forms because negative Laplace pressure in the meniscus initiates a pressure-gradient-driven capillary suction of oil from the flat film region. Due to the concave curvature of the oil surface, the pressure inside the meniscus is lower than in the flat film

Max Planck Institute for Polymer Research – Author's Manuscript

region. We calculate the pressure drop by the Young–Laplace equation $\Delta P = \gamma \left(\frac{1}{r_1} + \frac{1}{r_2}\right) =$ −78 Pa, where r_1 and r_2 are the radii describing the meniscus curvature (Fig. 1b, Supplemental Material). This equals to the hydrostatic pressure in water at a depth of ~8 mm.

In order to visualize the flow in the meniscus, we added polystyrene tracer particles to the silicone oil (Video S1). The capillary flow follows the oil–air interface. Here, viscous drag is negligible and the capillary flow strongest. Liquid flows up the meniscus until it turns downwards to compensate the meniscus growth at the perimeter (Fig. 1b, Fig. S2, Video S2, Video S3).

To demonstrate that capillary suction is a generic phenomenon we placed a piece of glass (Fig. 1c) or a silica sphere (25 µm diameter, Fig. S3) into the film and observed the flow in the oil. Right after placing the glass edge into the film, the oil is drawn towards the vertical wall and forms a meniscus. A circulative convection was observed in the meniscus around the glass (Video S4), similar to the meniscus around the water drop. The film depletion adjacent to the meniscus continues for as long as there is a pressure difference between the meniscus and the film region. Balancing the pressure difference can take several hours – or even days as shown with the meniscus around the piece of glass in Fig. 1c – depending on the geometry of the system and viscosity of the liquid (Supplemental Material, Fig. S4 and Fig. S5).

Max Planck Institute for Polymer Research – Author's Manuscript

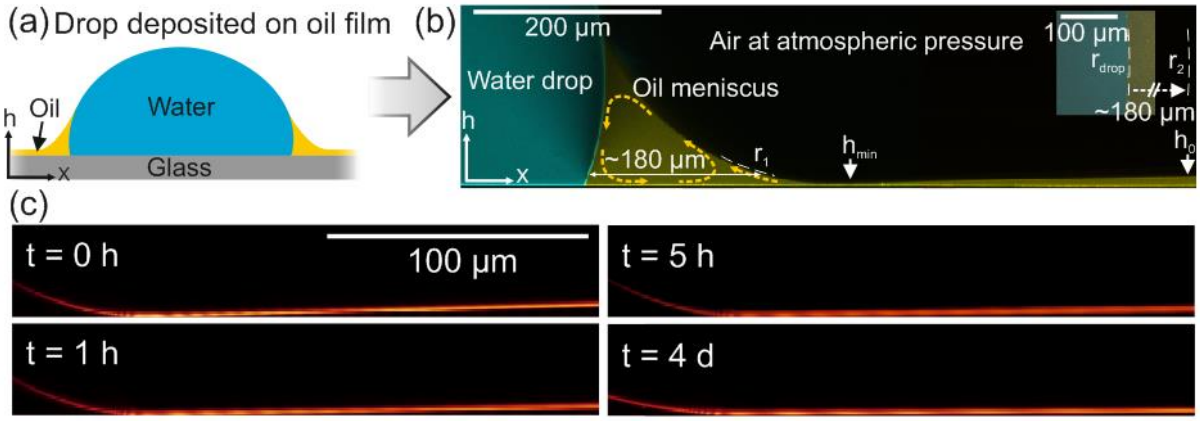

FIG. 1. Silicone oil meniscus and the oil film around a water drop or a piece of glass on a smooth glass substrate. (a) Illustration of a water drop deposited on the oil film. (b) A confocal microscopy image compiled from individual vertical micrographs in xh-plane (side-view) shows a 0.5 µL water drop (cyan, fluorescently dyed with WS-PDI) resting on a silicone oil film (yellow, dyed with Coumarin 6, initial film thickness $h_0 \approx 10$ µm) on glass. The micrographs were captured 1–2 min after placing the drop on the oil film. Yellow dotted arrows demonstrate circulative convection of the oil within the meniscus. r_1 corresponds to the vertical radius of the meniscus at ~10 µm height. Inset: top-view image (horizontal slice), where r_{drop} and r_2 correspond to the horizontal radius of the drop and the oil meniscus at ~10 µm height, respectively. (c) Confocal microscope reflection images of the meniscus (on the left-hand side of the minimum) and the depletion zone in xh-plane few minutes, 1 h, 5 h, and 4 days after placing a piece of glass (3×3×1 mm^3) on the oil film $h_0 \approx 8$ µm. The imaging position was adjusted to follow the depletion zone during growth of the meniscus.

To quantify dynamic wetting phenomena ahead of a moving water front we used a rectangular flow cell having a glass bottom surface and plastic side and top walls (Fig. 2a and Fig. S6). If not stated otherwise, confocal microscope observations were performed in the middle of the horizontal flow cell (with respect to x and y directions) to avoid corner effects. Prior to applying the water flow we wetted all walls of the flow cell with a thin silicone oil film $h_0 \approx$

Max Planck Institute for Polymer Research – Author's Manuscript

11 µm (η = 50 mPa s) by letting an oil plug move through the cell by gravity at 60° inclination angle (see Experimental Section and Fig. S7).

When water is driven into the flow cell, it accumulates an oil plug in the front. The oil plug has a concave curved meniscus covering all walls of the cell as shown in the representative examples in Fig. 2b and Fig. S6. The velocity of the oil meniscus was $v \approx 15$ µm/s corresponding to $Ca \approx 3.6\times10^{-5}$. Ahead of the meniscus the oil film adapts a curved profile with a local minimum $h_{min} \approx 3.5$ µm and a maximum $h_{max} \approx 17$ µm in film thickness. The minimum and the maximum are pushed forward by the oil meniscus (Fig. 2c, Video S5).

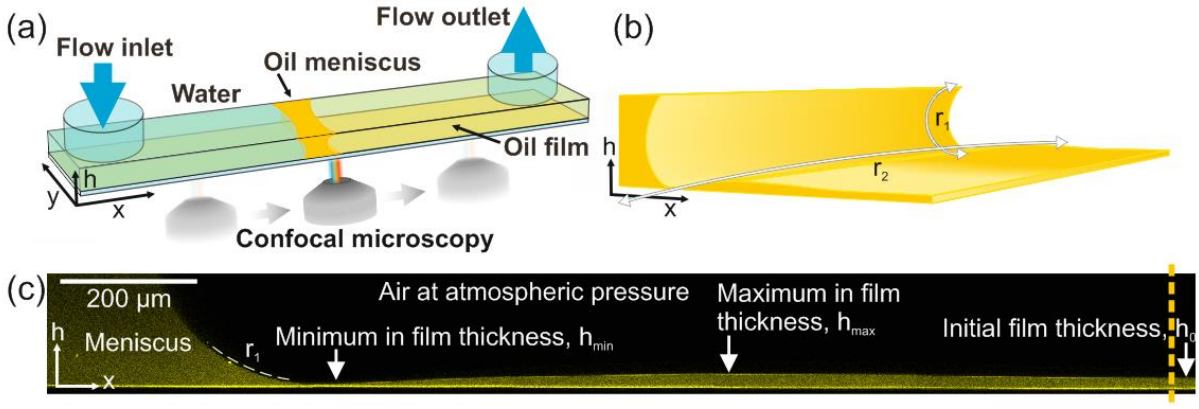

FIG. 2. Water advancing over the pre-existing silicone oil film in the flow cell. (a) Schematic illustration of the flow cell (length, x = 17 mm; width, y = 3.8 mm; height, h = 0.5 mm) setup on the confocal microscope. The oil meniscus ahead of water front is driven to the right. (b) Schematic drawing of the advancing oil meniscus and the film profile in the middle of the cell. r_1 and r_2 indicate curvature of the meniscus. (c) A confocal microscopy image compiled from individual vertical micrographs in xh-plane (side-view) shows the meniscus and the film profile advancing in the flow cell at $v \approx 15$ µm/s ($h_0 \approx 11$ µm, $h_{min} \approx 3.5$ µm, and $h_{max} \approx 17$ µm). The micrograph reveals approximately 1/3 (~170 µm) of the total height of the flow cell. Time resolution for the confocal microscopy was 0.85 s.

Max Planck Institute for Polymer Research – Author's Manuscript

The oil meniscus is characterized by two radii (Fig. 2b,c): a vertical radius $r_1 \approx -190$ µm and a horizontal radius $r_2 \approx -1100$ µm. The Young–Laplace equation predicts a pressure drop ΔP over the curved meniscus ≈ -130 Pa. The front of the advancing meniscus forms the local minimum in film thickness h_{min} by this pressure-gradient-driven capillary suction. When the oil meniscus moves forward, liquid in the film region enters the meniscus through this minimum. The minimum acts as a bottle neck for the liquid flow. To fulfill mass and momentum conservation, the liquid is piled up at h_{max} and a convex curvature in the film ahead of the minimum is formed. This increases the pressure gradient over h_{min} (Fig. 3).

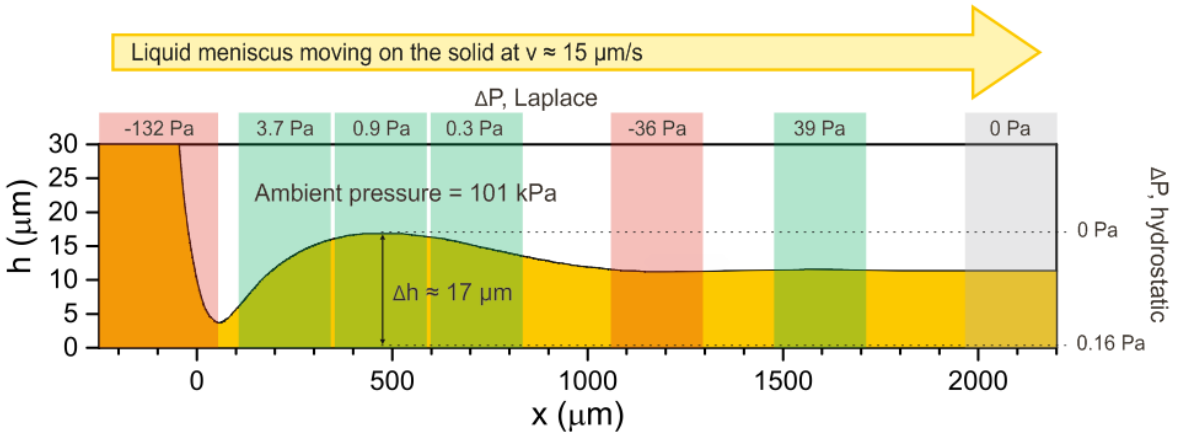

FIG. 3. Approximated Laplace and hydrostatic pressures acting at the silicone oil meniscus η = 50 mPa s and the curved oil film while advancing in the flow cell at $v \approx 15$ µm/s. Curvature of the oil meniscus is characterized by two negative radii (Fig. 2), vertical $r_1 \approx -190$ µm and horizontal $r_2 \approx -1100$ µm yielding approximated Laplace pressure of –132 Pa. Elsewhere in the film the effect of r_2 is considered to be negligible, thus the curvature r_1 determines the Laplace pressure at the given areas from left to right in the image as follows (calculated Laplace pressure, related curvature r_1): 3.7 Pa, 5700 µm; 0.9 Pa, 24000 µm; 0.3 Pa, 60000 µm; –36 Pa, –590 µm; 39 Pa, 540 µm. At the smooth film region, where the curvature of the oil interface is zero, the Laplace pressure is zero.

Max Planck Institute for Polymer Research – Author's Manuscript

In steady state the pressure gradient over h_{min} and the viscous forces in the liquid balance. To check that such a steady state exists, we recorded the film profile at different positions, and accordingly at different times, in the flow cell (Fig. 2a). Within the experimental error, the film profile remained unchanged (Experimental Section). When stopping movement of the meniscus the maximum in film thickness h_{max} disappeared while the minimum h_{min} remained for at least 60 min (Fig. 4).

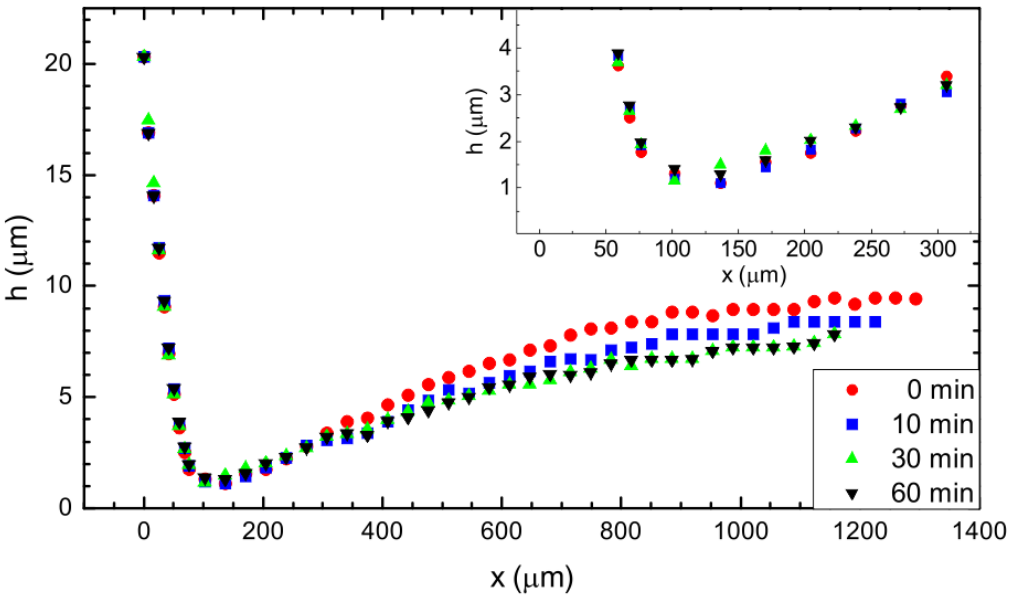

FIG. 4. Silicone oil meniscus η = 50 mPa s at rest in the flow cell. When stopping movement of the meniscus, the local minimum film height h_{min} in front of the meniscus and the concave curvature remained constant over the follow-up period of 60 min. Inset: magnification of the film profile at h_{min}. The gradual decrement of the film height can be associated with the capillary suction of the liquid in the meniscus of the oil plug and in the menisci at the walls of the flow cell.

From now on, we call the local minimum h_{min} and the maximum h_{max} ahead of the meniscus (Fig. 5a) a "primary minimum" and a "primary maximum", respectively, since there exist another, less prominent "secondary minimum" and "secondary maximum" advancing in the

Max Planck Institute for Polymer Research – Author's Manuscript

front (Fig. 5a, inset). The lower curvature of the liquid interface causes lower pressure drop and capillary suction: ΔP over the primary and secondary minima ≈ –132 Pa and ≈ –36 Pa, respectively (Fig. 3). The lateral distance between the secondary minimum and maximum, i.e. the width of half-wavelength *W*, appears to be similar to that of the primary minimum and maximum ≈ 400 µm. However, the amplitude *A*, i.e. the height difference between the minimum and the maximum is much smaller, ~1 µm.

To distinguish the effect of viscous forces, ηv, with respect to capillary forces, γ, on the film profile, we measured the half-wavelength and amplitude between the primary minimum and maximum at varying Ca ($3.9\times10^{-6} \leq Ca \leq 6.9\times10^{-4}$, Fig. 5a–c) and initial film thickness h_0. Both *W* and *A* increase linearly with h_0 (Fig. 5d,e). When increasing the velocity of the meniscus from ~15 µm/s to ~290 µm/s both *W* and *A* decrease (Fig. S8). The reason is that h_{min} has no time to evolve when the water front moves fast. Particularly, at $Ca < 10^{-4}$, where the capillary forces become increasingly important with respect to the viscous stresses, there is a threshold where both *W* and *A* start to increase greatly with decreasing Ca (Fig. 5f,g).

We compared the dynamic menisci ahead of moving water front (Fig. S1a) to those in dip-coating when a solid plate is withdrawn from or driven back into a liquid bath (Fig. S1b, dip-coating; Fig. S1c, "reverse dip-coating"). There the receding meniscus leaves behind a so-called "LLD" film [1,30] of thickness h_0, firstly analyzed by Landau and Levich [31] and Derjaguin [32]. The flow in the film region is determined by the interplay of viscous forces and capillarity, and is described within the lubrication approximation [3,31-36] assuming small curvature of the liquid–air interface and $Ca \ll 1$. Dynamic menisci were further investigated in a capillary tube by Bretherton [37].

Max Planck Institute for Polymer Research – Author's Manuscript

In the classic Landau–Levich–Bretherton (LLB) model [34] employed in dip-coating and reverse dip-coating, a balance of the viscous and capillary forces within the fluid layer yield the thin-film equation for the scaled film thickness $H = h/h_0$:

$$\frac{\mathrm{d}^3 H}{\mathrm{d}X^3} = \frac{H-1}{H^3}. \tag{1}$$

Here, X is a characteristic scale $X = x/\lambda$, with $\lambda = h_0 \left(\frac{\gamma}{-v3\eta}\right)^{1/3}$. The sign for the velocity of the meniscus is taken negative corresponding to a "reverse dip-coating scenario". Strictly the only formal requirement for validity of the above lubrication approximation is $Ca \ll 1$. For small variations in the film thickness ($H(X) = 1+\epsilon(X)$ with $\epsilon(X) \ll 1$), equation (1) has the 0th order solution

$$h(X) = h_0 \left[1 + C\, e^{-\frac{X}{2}} \cos\left(\frac{\sqrt{3}}{2}\, X\right)\right], \tag{2}$$

with a constant C to be determined. In this classic case, the film profile exhibits regular waves of constant half-wavelength $\omega = 2\pi\lambda/\sqrt{3}$.

Our measurements show that only the case with the largest capillary number $Ca = 6.9\times10^{-4}$ (η = 50 mPa s, v = 270 µm/s) exhibits such regular waves (Fig. 5c). In all other cases, the wavelength is not constant along x. Additionally, with decreasing Ca the experimental half-wavelength W measured between the first minimum and first maximum becomes smaller than the Landau–Levich half-wavelength ω.

Max Planck Institute for Polymer Research – Author's Manuscript

Correspondingly, the classic Landau-Levich-Bretherton theory can only capture the film profile in the case of the largest capillary number Ca = 6.9×10^{-4}. Fitting the experimental data with equation (2) yields a good match (Fig. 5c). The fit was performed in Mathematica with h_0 and ω being obtained from the experimental data. With decreasing Ca, the classic theory can only capture the film profile at large x (Fig. 5b and Fig. S9).

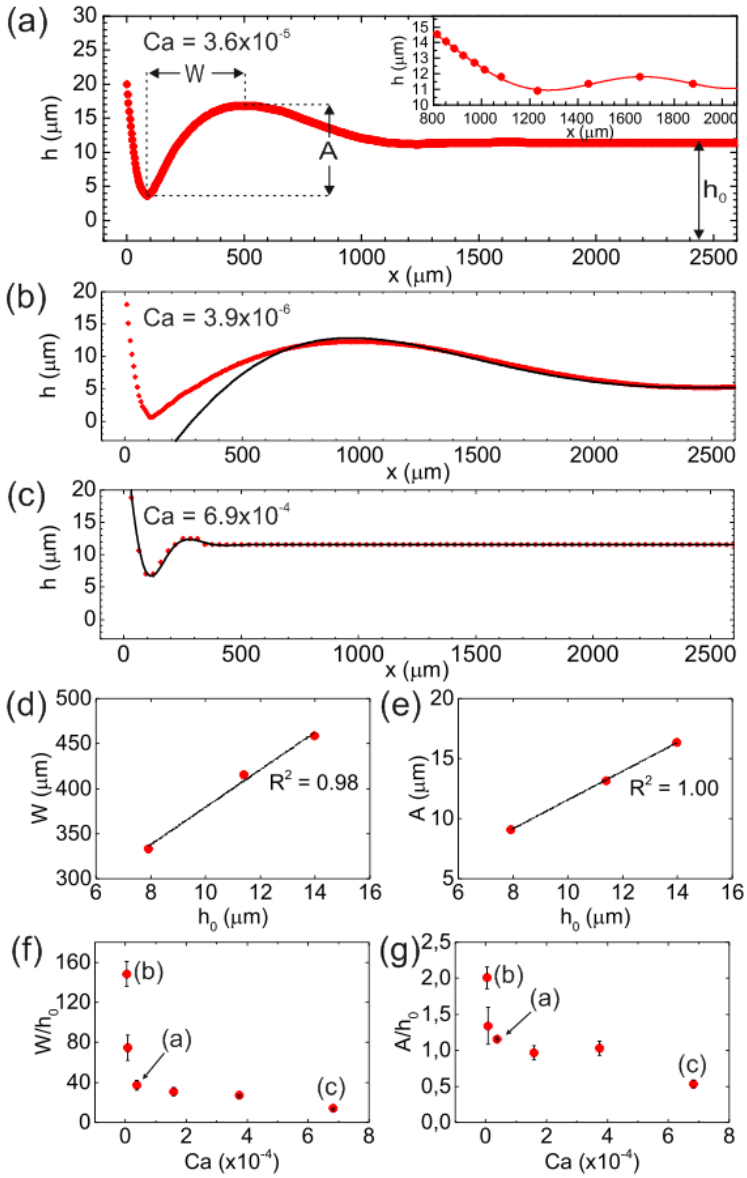

FIG. 5. Characterization of advancing silicone oil meniscus and the oil film profile in the flow cell. (a) Oil meniscus η = 50 mPa s advancing at $v \approx$ 15 µm/s (Ca = 3.6×10^{-5}) over the oil film $h_0 \approx$ 11 µm. *W* and *A* denote the half-wavelength and amplitude, respectively, of the primary

Max Planck Institute for Polymer Research – Author's Manuscript

minimum and maximum. Inset: magnification of the secondary minimum and maximum (red solid line is to guide eye). Film profile and theoretical fit (black solid line) with (b) the lowest ($v \approx 14$ µm/s, $\eta = 5$ mPa s, $Ca = 3.9\times10^{-6}$) and (c) the highest ($v \approx 290$ µm/s, $\eta = 50$ mPa s, $Ca = 6.9\times10^{-4}$) investigated capillary numbers. The confocal microscopy time resolution for (a), (b), and (c) was 0.217, 0.530, and 0.109 s, respectively. (d) W and (e) A are linearly dependent on h_0 ($v \approx 15$ µm/s, $\eta = 50$ mPa s, $Ca = 3.6\times10^{-5}$). (f) W and (g) A decrease with increasing Ca (a, b, and c refer to the film profiles at the corresponding Ca).

The model within the Landau–Levich–Bretherton framework predicts a constant spacing between the minima and maxima for all x. Notably, a decreasing/increasing spacing occurs with decreasing capillary number. Experimentally, for $Ca = 3.6\times10^{-5}$ (Fig. 5a) the spacing between the primary minimum and maximum was about 40% less than spacing between the maximum and the secondary minimum. When the velocity of the meniscus is reduced to zero ($Ca = 0$), the characteristic half-wavelength W/h_0 should go $\rightarrow \infty$, in agreement with our data, Fig. 5f. Our setup rules out that gravitational drainage could cause the discrepancy between theoretical predictions and experimental observations [35] as the flow cell was horizontally aligned.

To find the reason for the discrepancy between theory and experiments for $Ca < 6\times10^{-4}$ we measured local flow in the oil film by imaging movement of the tracer particles (Figs. 6a, 7, S10). In front of the minima in film thickness (Fig. 6b for the primary minimum and Fig. 6c for the secondary minimum) the tracer particles have a positive velocity with respect to the flow direction of the meniscus. Notably, when the minima are approaching the particles, the flow slows down before the particles experience a negative velocity when sucked through the minima. The maximum horizontal backflow velocities of the tracer particles were −73 µm/s (Fig. 6b, Video S6) and −2 µm/s (Fig. 6c, Video S7) at the primary and the secondary

Max Planck Institute for Polymer Research – Author's Manuscript

minimum in film thickness, respectively. That is, the maximum backflow velocity equals 5 times the velocity of the oil meniscus.

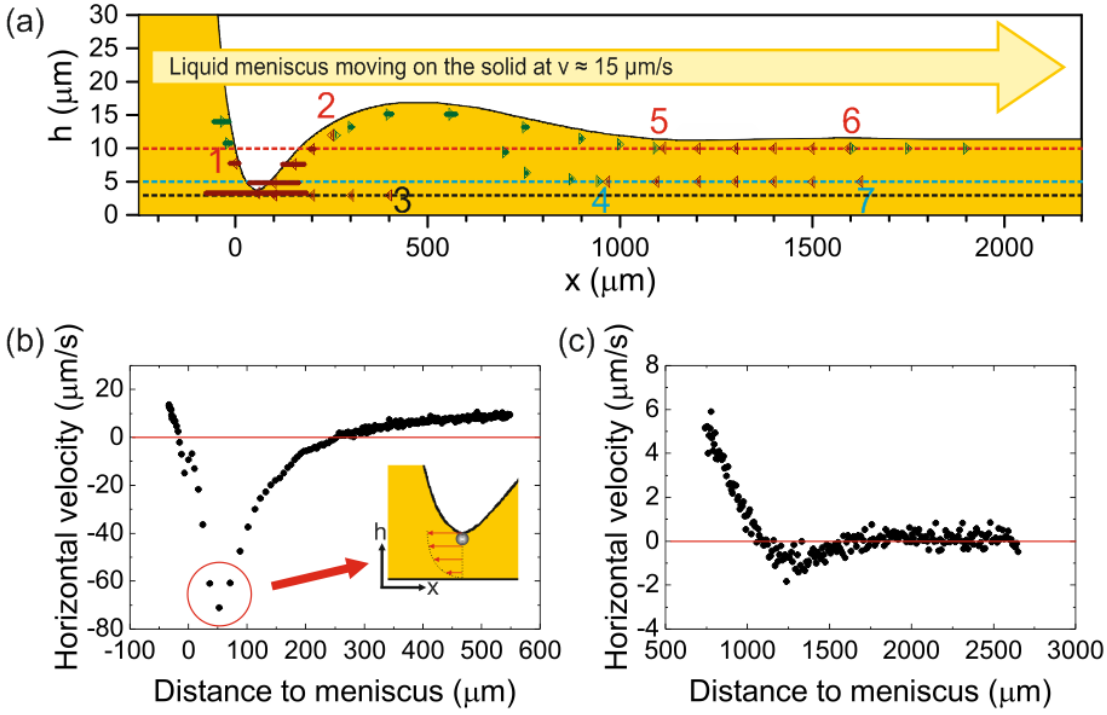

FIG. 6. Hydrodynamic flow of silicone oil meniscus η = 50 mPa s advancing at $v \approx 15$ μm/s over a pre-existing oil film h_0 = 11 μm. (a) Illustration of flow in the oil based on confocal microscopy data collected at different regions in the film from several individual experiments. The film profile was captured from the reflection images in xh-plane (side-view). The horizontal velocity and vertical motion of the tracer particles were monitored in transmission (Fig. S10) and fluorescence (Fig. 7) images in xy-plane (top-view) with a time resolution of 0.217 s. Length of the green and red arrows denote magnitude of positive and negative horizontal velocity, respectively, of the tracer particles at the given positions. The data was collected by setting the focal plane at the heights of 3.5, 5, and 10 μm above the glass substrate, indicated by the dashed lines. (b) Backflow over the primary minimum (turning points 1–3 in (a)) and (c) backflow over the secondary minimum (turning points 4–7 in (a)).

Max Planck Institute for Polymer Research – Author's Manuscript

Inset in (b): illustration of the backflow transporting a tracer particle through the primary minimum.

We identified 7 positions at different heights in the oil film, labelled 1–7 in Fig. 6a, where the flow direction switched. These "turning points" are associated with the two backflows. Before changing the flow direction, the oil has lower positive velocity close to the solid (no-slip condition at the solid–liquid interface) as compared to the liquid–air interface (negligible friction). Therefore, the backflows start earlier and are longer at the heights of 3.5 and 5 µm as compared to the height at 10 µm (Fig. 6a, Fig. 7 and Supplemental Material, Table SI). After entering the meniscus, the flow turns back to positive and starts to follow the motion of the meniscus. This hints that the strong backflows within the liquid film cause the discrepancy between theory and experiments.

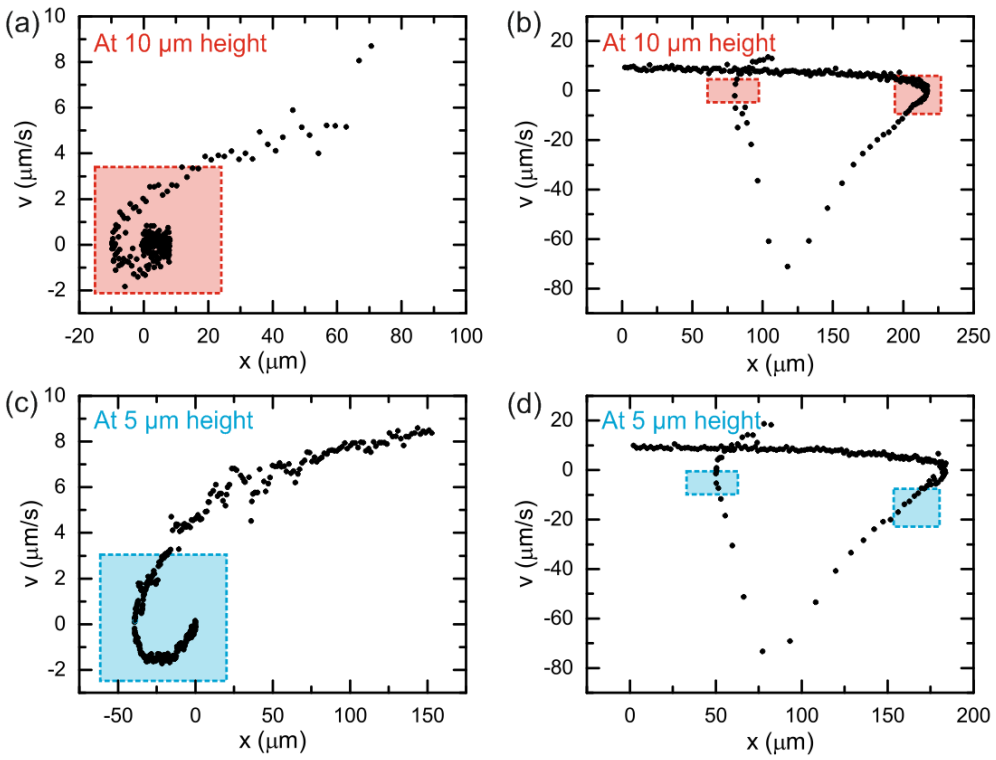

FIG. 7. Hydrodynamic flow at different heights in the silicone oil film. Oil viscosity η = 50 mPa s, meniscus velocity $v \approx 15$ µm/s, and initial film thickness h_0 = 11 µm. The coordinates

Max Planck Institute for Polymer Research – Author's Manuscript

of 1 μm polystyrene tracer microparticles in the oil film were monitored by confocal microscopy. The data was collected with the focal plane set at 10 and 5 μm above the glass substrate using the confocal microscope transmission channel. The data reveals two backflows in the film: a, c) over the secondary minimum and b, d) over the primary minimum in film thickness. a, b) Red and c, d) blue rectangles correspond to the data acquired at ~10 ± 1 μm and ~5 ± 1 μm heights in the film, respectively, using the confocal microscope fluorescent channel.

The capillary suction discussed here was observed for different thicknesses of the film (Fig. S4) and viscosities of the liquid (Fig. S5). It is expected to have broad implications in technology. One example is the common problem of inhomogeneous formation of coating films – also known as the "orange peel effect" – in painting, lacquering, and other thin-film coating applications [38]. Small microscale defects can cause considerably large variation in film thickness even at mm-wide areas (Fig. S3). The capillary suction and film depletion should also be apparent in a standard dip-coating process (Fig. S1b).

Getting back to the pitcher plant and lubricant-infused slippery surfaces; when a 0.5 μL water drop surrounded by open air slides on a thin silicone oil film (η = 50 mPa s, $h_0 \approx 8$ μm) on a PDMS modified glass slide [24] (Experimental Section) – consistent with the observations in the flow cell – a minimum and a maximum in film thickness are formed ahead of the annular wetting ridge surrounding the drop. Inclination of the substrate by 4° caused a downward motion of the drop at a velocity of ~70 μm/s. Here, the minimum and maximum in film thickness became ~3 μm and ~10 μm, respectively (Video S8).

Max Planck Institute for Polymer Research – Author's Manuscript

III. Conclusions

In summary, we investigate the wetting dynamics of one liquid (water) front advancing over a micrometer-thick film of another immiscible liquid (silicone oil). The novel experimental setup with confocal microscopy and tracer microparticles within the liquid provides information of the shape of the liquid surface and of the flow within the micrometer-thick oil film. A negative Laplace pressure in the liquid meniscus leads to capillary suction and as a consequence a local thinning of the liquid film ahead of the advancing meniscus. The lubrication approximation theory within Landau–Levich–Bretherton framework can describe the dynamic film profile for Ca of the order of 6×10^{-4}. It cannot predict the film profile at lower Ca where strong capillary-suction-induced backflows occur. Capillary forces can initiate strong pressure drops – and thus significantly change the flow and profile of thin liquid films – around solid particles, walls, or drops of immiscible liquids.

IV. Experimental Section

Materials: Silicone oils were purchased from Sigma-Aldrich (Germany). The flow in thin oil films was investigated at varying capillary numbers (Ca) with different flow velocities and viscosities of the oils (η = 5 mPa s, γ = 18.1 ± 0.2 mN/m; η = 10 mPa s, γ = 18.9 ± 0.3 mN/m; η = 50 mPa s, γ = 20.9 ± 0.5 mN/m; η = 500 mPa s, γ = 22.7 ± 0.2 mN/m). If not otherwise mentioned, the silicone oil with η = 50 mPa s was used. Interfacial tension between the oil and water, γ_{OW}, is 38.9 ± 0.3 mN/m. Hydrophobic fluorescent dye, Coumarin 6 with the concentration of 50 µg/g, was used to label the silicone oil. Prior to the experiments, the dyed oil was sonicated for 2 h and filtered through a 0.22 µm syringe filter to remove possible aggregates of the dye. To monitor flow inside the oil film, 1 µm diameter polystyrene tracer particles were added to the oil at a concentration of 10 µg/g. Water drops (de-ionized MilliQ

Max Planck Institute for Polymer Research – Author's Manuscript

water, γ = 73.0 ± 0.2 mN/m, η = 1 mPa s, ρ = 1.00 g/mL) resting on or moving over the pre-existing liquid films of silicone oils were labeled with a hydrophilic fluorescent dye, N,N′-(2,6-diisopropylphenyl)-1,6,7,12-tetra(1-methylpyridinium-3-yloxy)-perylene-3,4,9,10-tetracarboxylic acid diimide tetra-methane-sulfonate (WS-PDI), with a concentration of 10 µg/g. With the used concentrations, the effect of dyes on the surface tension of the silicone oil and water, or the interfacial tension between the oil and water, was negligible and remained within the experimental error of 0.5 mN/m.

Surface and interfacial tensions: Surface tensions of the liquids were measured using the Wilhelmy plate method with DCAT 11 -tensiometer (DataPhysics Instruments GmbH, Germany). Interfacial tensions between the liquids were measured by DataPhysics OCA 35 instrument using the pendant drop method (DataPhysics Instruments GmbH, Germany).

Confocal microscopy: Inverted laser scanning confocal microscope (LSCM, Leica TCS SP8 SMD, Leica Microsystems GmbH, Germany) was used to investigate the profile and hydrodynamics of the silicone oil menisci and the oil films. The confocal microscope was equipped with a water immersion objective (40× magnification) with horizontal and vertical resolution of ~500 nm and ~1 µm, respectively. Argon laser lines 458 nm and 476 nm were used for reflection at interfaces and for excitation of Coumarin 6 dye, respectively. DPSS laser line 561 nm was used to excite WS-PDI dye. Five individual detectors with freely adjustable spectral ranges allow simultaneous measurement of emitted light from the dyes (emission peak at 488 nm for Coumarin 6 and at 609 nm for WS-PDI), reflected light from the interfaces, and transmitted light through the sample.

Meniscus around a drop, a solid sphere, and a glass piece: To investigate the evolution of the oil meniscus outside the flow cell in open air around a water drop, in front of a piece of glass,

Max Planck Institute for Polymer Research – Author's Manuscript

or around silica particles having a diameter of 25 µm (AkzoNobel, Kromasil, Sweden), we deposited 1 µL of silicone oil, η = 50 mPa s or η = 5 mPa s, on the glass substrate and spin-coated the sample at 1000 rpm or 200 rpm, respectively, for 60 s. This resulted in a smooth film of oil with thickness ~8–10 µm. With silicone oil η = 50 mPa s we achieved a thick film of ~100 µm (Fig. S4) by letting a 1 µL drop of the oil spontaneously spread on the glass substrate. Monitoring hydrodynamics within the oil meniscus was started immediately after placing the water drop, the piece of glass, or the silica particles on the oil film and focusing at the area of interest, typically within 1–2 minutes.

Flow cell: Commercial flow cells, sticky-Slide VI$^{0.4}$ from ibidi (Germany), were used to investigate the dynamic menisci under well-defined conditions in horizontal plane. The flow cells (length = 17 mm; width = 3.8 mm; height = 0.5 mm) are made of high optical quality plastic, are closed from the top, and can be attached to the substrate by a self-adhesive underside. Microscope coverslip glass with a thickness of 170 µm (Thermo Fisher Scientific, Germany), cleaned with ethanol, rinsed with MilliQ water, and dried under a nitrogen flow, was used as a substrate. The glass substrate was firmly attached to the flow cell and ~0.5 µL of silicone oil was deposited in the flow cell from the inlet. The film thickness was controlled by adjusting the tilting angle: ~60° tilt angle yielded a film thickness $h_0 \approx 11$ µm along the center line of the flow channel. After the film formation, an inlet tube for water flow was connected to the flow cell. A pressure generated while connecting the tube punctured the oil plug at the outlet of the flow cell. During the experiments the oil film was under atmospheric pressure. Water flow was driven into the flow cell by a peristaltic pump (Reglo Analog MS-4/8, Ismatec, Germany) connected to a poly(vinyl chloride) tube with inner diameter of 0.13 mm. This tube was further connected to a wider tube with inner diameter of 1.37 mm to eliminate possible velocity fluctuations originating from the pump. Velocity of the oil meniscus in the flow cell was determined for each individual experiment by direct confocal

Max Planck Institute for Polymer Research – Author's Manuscript

microscopy observation, i.e. the length the meniscus advanced was divided by the elapsed time.

Water drop sliding on a slippery surface: To investigate a meniscus around a sliding water drop on a silicone oil coated slippery surface, the glass substrate was treated following a simple procedure that results in a nm-thick hydrophobic PDMS brush coating [24]. Briefly, the glass was first cleaned with ethanol and water and dried under nitrogen flow. 5 µL of silicone oil η = 50 mPa s was deposited on the glass after which the sample was heated on a hot plate at 300°C for ~3 min. After the heat treatment, the sample was rinsed with tetrahydrofuran and water. 1 µL drop of silicone oil η = 50 mPa s was spin-coated on the surface at 1000 rpm for 60 s to achieve a smooth film of the oil with thickness of 8 µm. The sample was placed on the confocal microscope sample holder at a tilt angle of 4°. A 0.5 µL water drop was then placed on the inclined surface where it was imaged when sliding downwards.

Data analysis: Profile of the oil menisci and films were investigated by capturing the film profiles at xh-plane (side-view) at the center line of the flow cell and by monitoring dynamics of the polystyrene tracer particles within the oil at xy-plane (top-view) at different heights in the film by confocal microscopy. Image processing and data analysis was carried out using Fiji open-source platform for image analysis [39]. The curved oil film profiles were analyzed from sequentially recorded confocal microscopy images with a house-made Fiji macro, which was designed to distinguish the oil–air interface from changes in pixel intensity of the microscopy images.

From the quantitative data extracted from the confocal microscopy videos, the half-wavelength (W) and amplitude (A) were determined using at least 3 individual flow profiles to

Max Planck Institute for Polymer Research – Author's Manuscript

get the characteristic ratios W/h_0 and A/h_0 for the oil meniscus flows at different Ca. The flow profiles were typically acquired in the middle of the flow cell in x- and y-directions, Fig. 2a. We also characterized film profile for a single flow at a velocity of the oil meniscus $v \approx 15$ µm/s, η = 50 mPa s, and $Ca = 3.6\times10^{-5}$ in the front part of the flow cell and at the rear part of the cell to check that after reaching the equilibrium flow, the film maintained its profile unchanged ahead of the advancing meniscus. In the front part of the flow cell the ratios W/h_0 and A/h_0 were 32.8 and 1.17, respectively, and after the meniscus had advanced ~10 mm through the flow cell to its rear part the corresponding ratios remained unchanged within experimental error, being 36.4 and 1.16, respectively. Average for W/h_0 and A/h_0 measured from three individual flows at $Ca = 3.6\times10^{-5}$ were 37.1 ± 4.7 and 1.16 ± 0.01, respectively.

Curvature of the oil films was analyzed from the micrographs using ThreePointCircularROI – Fiji plugin [40] to evaluate the Laplace pressure difference over the curved oil interface at different positions. Hydrodynamics within the oil were investigated by analyzing the horizontal (x-directional) velocity of the tracer particles using Mosaic Particle Tracker 2D/3D –Fiji plugin [41]. In the fluorescent channel of the confocal microscope, the particles remained visible ca. ±1 µm with respect to the set focal plane, i.e. 10 ± 1 µm, 5 ± 1 µm, and 3.5 ± 1 µm (Fig. 6a). In the transmission channel the horizontal velocity of the tracer particles could be monitored independently on the changes in the height position of the particles. With the information received from the transmission channel, we could determine whether the particles moved upwards or downwards with respect to the set focal xy-plane. When the particle was above the focal plane, i.e. moved upwards, it became blurry with a bright center. When the particle was below the focal plane, i.e. moved downwards in the liquid film, it became blurry with a dark center (Fig. S10).

Max Planck Institute for Polymer Research – Author's Manuscript

Start and end positions for the local backflows within the oil film with respect to the meniscus position were calculated knowing the elapsed time, the distance covered by the backflow, and the velocity of the advancing meniscus (Table SI):

$$x_{start} = (t_{meniscus\ arrival} - t_{backflow\ start})v, \quad (3)$$

where $t_{meniscus\ arrival}$ is the time at which the meniscus passed the backflow start position, $t_{backflow\ start}$ is the time at which the backflow started, and v is the velocity of the oil meniscus.

The position where the backflow ends in relation to the position of the oil meniscus is given by

$$x_{end} = x_{start} - t_{backflow}v - l_{backflow}, \quad (4)$$

where $t_{backflow}$ is the duration and $l_{backflow}$ is the distance covered by the backflow.

To further verify the positions of the backflows with respect to the oil film curvature, we compared the reflection channel microscopy information from the oil−air interface, where the changes in the height of the film were detected, with the transmission channel information, where dynamics of the tracer particles were detected.

References

[1] J. H. Snoeijer, J. Ziegler, B. Andreotti, M. Fermigier, and J. Eggers, Thick films of viscous fluid coating a plate withdrawn from a liquid reservoir, Phys. Rev. Lett. **100**, 244502 (2008).

Max Planck Institute for Polymer Research – Author's Manuscript

[2] R. Krechetnikov and G. M. Homsy, Surfactant effects in the Landau–Levich problem, J. Fluid Mech. **559**, 429 (2006).

[3] K. Stoev, E. Ramé, T. Leonhardt, and S. Garoff, The effects of thin films on the hydrodynamics near moving contact lines, Phys. Fluids **10**, 1793 (1998).

[4] F. C. Krebs, Fabrication and processing of polymer solar cells: A review of printing and coating techniques, Sol. Energ. Mat. Sol. C. **93**, 394 (2009).

[5] C. E. Colosqui, J. F. Morris, and H. A. Stone, Hydrodynamically driven colloidal assembly in dip coating, Phys. Rev. Lett. **110**, 188302 (2013).

[6] W. H. Briscoe, S. Titmuss, F. Tiberg, R. K. Thomas, D. J. McGillivray, and J. Klein, Boundary lubrication under water, Nature **444**, 191 (2006).

[7] N. R. Morrow, Wettability and its effect on oil-recovery, J. Pet. Technol. **42**, 1476 (1990).

[8] J. Rubio, M. L. Souza, and R. W. Smith, Overview of flotation as a wastewater treatment technique, Miner. Eng. **15**, 139 (2002).

[9] W. Barthlott and C. Neinhuis, Purity of the sacred lotus, or escape from contamination in biological surfaces, Planta **202**, 1 (1997).

[10] X. Deng, L. Mammen, H.-J. Butt, and D. Vollmer, Candle soot as a template for a transparent robust superamphiphobic coating, Science **335**, 67 (2012).

[11] H. Teisala, M. Tuominen, and J. Kuusipalo, Superhydrophobic coatings on cellulose-based materials: fabrication, properties, and applications, Adv. Mater. Interfaces **1**, 1300026 (2014).

[12] A. W. Neumann, A. H. Abdelmessih, and A. Hameed, The role of contact angles and contact angle hysteresis in dropwise condensation heat transfer, Int. J. Heat Mass Transfer **21**, 947 (1978).

[13] G. Azimi, R. Dhiman, H. M. Kwon, A. T. Paxson, and K. K. Varanasi, Hydrophobicity of rare-earth oxide ceramics, Nat. Mater. **12**, 315 (2013).

Max Planck Institute for Polymer Research – Author's Manuscript

[14] S. Anand, A. T. Paxson, R. Dhiman, J. D. Smith, and K. K. Varanasi, Enhanced condensation on lubricant-impregnated nanotextured surfaces, ACS Nano **6**, 10122 (2012).

[15] K.-C. Park, P. Kim, A. Grinthal, N. He, D. Fox, J. C. Weaver, and J. Aizenberg, Condensation on slippery asymmetric bumps, Nature **531**, 78 (2016).

[16] Y. Zheng, H. Bai, Z. Huang, X. Tian, F. Q. Nie, Y. Zhao, J. Zhai, and L. Jiang, Directional water collection on wetted spider silk, Nature **463**, 640 (2010).

[17] N. R. Tas, P. Mela, T. Kramer, J. W. Berenschot, and A. van den Berg, Capillarity induced negative pressure of water plugs in nanochannels, Nano Lett. **3**, 1537 (2003).

[18] J. E. McDonald and S. Brubaker, Meniscus-induced thinning of tear films, Am. J. Ophthalmol. **72**, 139 (1971).

[19] A. Sharma, S. Tiwari, R. Khanna, and J. M. Tiffany, in *Lacrimal Gland, Tear Film, and Dry Eye Syndromes 2*, edited by D. A. Sullivan, D. A. Dartt, and M. A. Meneray (Plenum Press, New York, 1998), pp. 425.

[20] H. F. Bohn and W. Federle, Insect aquaplaning: Nepenthes pitcher plants capture prey with the peristome, a fully wettable water-lubricated anisotropic surface, Proc. Natl. Acad. Sci. U.S.A. **101**, 14138 (2004).

[21] E. Spruijt, E. Le Guludec, C. Lix, M. Wagner, and D. Quéré, Liquid filmification from menisci, Europhys. Lett. **112**, 16002 (2015).

[22] T. S. Wong, S. H. Kang, S. K. Tang, E. J. Smythe, B. D. Hatton, A. Grinthal, and J. Aizenberg, Bioinspired self-repairing slippery surfaces with pressure-stable omniphobicity, Nature **477**, 443 (2011).

[23] J. D. Smith, R. Dhiman, S. Anand, E. Reza-Garduno, R. E. Cohen, G. H. McKinley, and K. K. Varanasi, Droplet mobility on lubricant-impregnated surfaces, Soft Matter **9**, 1772 (2013).

Max Planck Institute for Polymer Research – Author's Manuscript

[24] A. Eifert, D. Paulssen, S. N. Varanakkottu, T. Baier, and S. Hardt, Simple fabrication of robust water-repellent surfaces with low contact-angle hysteresis based on impregnation, Adv. Mater. Interfaces **1**, 1300138 (2014).

[25] F. Schellenberger, J. Xie, N. Encinas, A. Hardy, M. Klapper, P. Papadopoulos, H.-J. Butt, and D. Vollmer, Direct observation of drops on slippery lubricant-infused surfaces, Soft Matter **11**, 7617 (2015).

[26] N. MacCallum *et al.*, Liquid-infused silicone as a biofouling-free medical material, ACS Biomater. Sci. Eng. **1**, 43 (2015).

[27] J. S. Wexler, I. Jacobi, and H. A. Stone, Shear-driven failure of liquid-infused surfaces, Phys. Rev. Lett. **114**, 168301 (2015).

[28] D. Daniel, J. V. I. Timonen, R. Li, S. J. Velling, and J. Aizenberg, Oleoplaning droplets on lubricated surfaces, Nat. Phys. **13**, 1020 (2017).

[29] M. Nosonovsky, Slippery when wetted, Nature **477**, 412 (2011).

[30] J. Eggers, Hydrodynamic theory of forced dewetting, Phys. Rev. Lett. **93**, 094502 (2004).

[31] L. Landau and B. Levich, Dragging of a liquid by a moving plate, Acta Physicochim. URSS **17**, 42 (1942).

[32] B. V. Derjaguin, On the thickness of a layer of liquid remaining on the walls of vessels after their emptying, and the theory of the application of photoemulsion after coating on the cine film, Acta Physicochim. URSS **20**, 349 (1943).

[33] H. A. Stone, Interfaces: in fluid mechanics and across disciplines, J. Fluid Mech. **645**, 1 (2010).

[34] R. F. Probstein, *Physicochemical Hydrodynamics: An Introduction* (Wiley Interscience, New York, 2003), 2. edn.

[35] M. Maleki, M. Reyssat, F. Restagno, D. Quéré, and C. Clanet, Landau-Levich menisci, J. Colloid Interface Sci. **354**, 359 (2011).

Max Planck Institute for Polymer Research – Author's Manuscript

[36] X. Chen, E. Ramé, and S. Garoff, The effects of thin and ultrathin liquid films on dynamic wetting, Phys. Fluids **16**, 287 (2004).

[37] F. P. Bretherton, The motion of long bubbles in tubes, J. Fluid Mech. **10**, 166 (1961).

[38] A. Abbasian, S. R. Ghaffarian, N. Mohammadi, M. R. Khosroshahi, and M. Fathollahi, Study on different planforms of paint's solvents and the effect of surfactants (on them), Prog. Org. Coat. **49**, 229 (2004).

[39] J. Schindelin *et al.*, Fiji: an open-source platform for biological-image analysis, Nat. Methods **9**, 676 (2012).

[40] G. Landini, ThreePointCircularROI (ImageJ plugin), www.mecourse.com/landinig/software/software.html (2016).

[41] I. F. Sbalzarini and P. Koumoutsakos, Feature point tracking and trajectory analysis for video imaging in cell biology, J. Struct. Biol. **151**, 182 (2005).

Acknowledgments

This work was funded by the ERC advanced grant 340391 – SUPRO. D.V. acknowledges financial support from the European Union's Horizon 2020 research and innovation programme under the Marie Sklodowska-Curie grant agreement No 722497. H.T. acknowledges Tekes – the Finnish Funding Agency for Innovation (grant 40365/14 – ROLLIPS), Walter Ahlström Foundation (Tutkijat maailmalle –program), and Alexander von Humboldt Foundation for financial support. Gabriele Schäfer and Krzysztof Ciszewski are acknowledged for technical support. Dr. Holger Marschall is greatly acknowledged for stimulating discussion.

Max Planck Institute for Polymer Research – Author's Manuscript

Figure captions

FIG. 1. Silicone oil meniscus and the oil film around a water drop or a piece of glass on a smooth glass substrate. (a) Illustration of a water drop deposited on the oil film. (b) A confocal microscopy image compiled from individual vertical micrographs in xh-plane (side-view) shows a 0.5 µL water drop (cyan, fluorescently dyed with WS-PDI) resting on a silicone oil film (yellow, dyed with Coumarin 6, initial film thickness $h_0 \approx 10$ µm) on glass. The micrographs were captured 1–2 min after placing the drop on the oil film. Yellow dotted arrows demonstrate circulative convection of the oil within the meniscus. r_1 corresponds to the vertical radius of the meniscus at ~10 µm height. Inset: top-view image (horizontal slice), where r_{drop} and r_2 correspond to the horizontal radius of the drop and the oil meniscus at ~10 µm height, respectively. (c) Confocal microscope reflection images of the meniscus (on the left-hand side) and the depletion zone in xh-plane few minutes, 1 h, 5 h, and 4 days after placing a piece of glass (3×3×1 mm^3) on the oil film $h_0 \approx 8$ µm. The imaging position was adjusted to follow the depletion zone during growth of the meniscus.

FIG. 2. Water advancing over the pre-existing silicone oil film in the flow cell. (a) Schematic illustration of the flow cell (length, x=17 mm; width, y=3.8 mm; height, h=0.5 mm) setup on the confocal microscope. The oil meniscus ahead of water front is driven to the right. (b) Schematic drawing of the advancing oil meniscus and the film profile in the middle of the cell. r_1 and r_2 indicate curvature of the meniscus. (c) A confocal microscopy image compiled from individual vertical micrographs in xh-plane (side-view) shows the meniscus and the film profile advancing in the flow cell at $v \approx 15$ µm/s ($h_0 \approx 11$ µm, $h_{min} \approx 3.5$ µm, and $h_{max} \approx 17$ µm). The micrograph reveals approximately 1/3 (~170 µm) of the total height of the flow cell. Time resolution for the confocal microscopy was 0.85 s.

Max Planck Institute for Polymer Research – Author's Manuscript

FIG. 3. Approximated Laplace and hydrostatic pressures acting at the silicone oil meniscus η = 50 mPa s and the curved oil film while advancing in the flow cell at $v \approx 15$ µm/s. Curvature of the oil meniscus is characterized by two negative radii (Fig. 2), vertical $r_1 \approx -190$ µm and horizontal $r_2 \approx -1100$ µm yielding approximated Laplace pressure of –132 Pa. Elsewhere in the film the effect of r_2 is considered to be negligible, thus the curvature r_1 determines the Laplace pressure at the given areas from left to right in the image as follows (calculated Laplace pressure, related curvature r_1): 3.7 Pa, 5700 µm; 0.9 Pa, 24000 µm; 0.3 Pa, 60000 µm; –36 Pa, –590 µm; 39 Pa, 540 µm. At the smooth film region, where the curvature of the oil interface is zero, the Laplace pressure is zero.

FIG. 4. Silicone oil meniscus η = 50 mPa s at rest in the flow cell. When stopping movement of the meniscus, the local minimum film height h_{min} in front of the meniscus and the concave curvature remained constant over the follow-up period of 60 min. Inset: magnification of the film profile at h_{min}. The gradual decrement of the film height can be associated with the capillary suction of the liquid in the meniscus of the oil plug and in the menisci at the walls of the flow cell.

FIG. 5. Characterization of advancing silicone oil meniscus and the oil film profile in the flow cell. (a) Oil meniscus η=50 mPa s advancing at $v \approx 15$ µm/s (Ca=3.6×10^{-5}) over the oil film $h_0 \approx 11$ µm. *W* and *A* denote the half-wavelength and amplitude, respectively, of the primary minimum and maximum. Inset: magnification of the secondary minimum and maximum (red solid line is to guide eye). Film profile and theoretical fit (black solid line) with (b) the lowest ($v \approx 14$ µm/s, η=5 mPa s, Ca=3.9×10^{-6}) and (c) the highest ($v \approx 290$ µm/s, η=50 mPa s, Ca=6.9×10^{-4}) investigated capillary numbers. The confocal microscopy time resolution for (a), (b), and (c) was 0.217, 0.530, and 0.109 s, respectively. (d) *W* and (e) *A* are linearly

Max Planck Institute for Polymer Research – Author's Manuscript

dependent on h_0 ($v \approx 15$ μm/s, η=50 mPa s, Ca=3.6×10^{-5}). (f) W and (g) A decrease with increasing Ca (a, b, and c refer to the film profiles at the corresponding Ca).

FIG. 6. Hydrodynamic flow of silicone oil meniscus η=50 mPa s advancing at $v \approx 15$ μm/s over a pre-existing oil film h_0=11 μm. (a) Illustration of flow in the oil based on confocal microscopy data collected at different regions in the film from several individual experiments. The film profile was captured from the reflection images in xh-plane (side-view). The horizontal velocity and vertical motion of the tracer particles were monitored in transmission (Fig. S10) and fluorescence (Fig. 7) images in xy-plane (top-view) with a time resolution of 0.217 s. Length of the green and red arrows denote magnitude of positive and negative horizontal velocity, respectively, of the tracer particles at the given positions. The data was collected by setting the focal plane at the heights of 3.5, 5, and 10 μm above the glass substrate, indicated by the dashed lines. (b) Backflow over the primary minimum (turning points 1–3 in (a)) and (c) backflow over the secondary minimum (turning points 4–7 in (a)). Inset in (b): illustration of the backflow transporting a tracer particle through the primary minimum.

FIG. 7. Hydrodynamic flow at different heights in the silicone oil film. Oil viscosity η = 50 mPa s, meniscus velocity $v \approx 15$ μm/s, and initial film thickness h_0 = 11 μm. The coordinates of 1 μm polystyrene tracer microparticles in the oil film were monitored by confocal microscopy. The data was collected with the focal plane set at 10 and 5 μm above the glass substrate using the confocal microscope transmission channel. The data reveals two backflows in the film: a, c) over the secondary minimum and b, d) over the primary minimum in film thickness. a, b) Red and c, d) blue rectangles correspond to the data acquired at ~10 ± 1 μm and ~5 ± 1 μm heights in the film, respectively, using the confocal microscope fluorescent channel.